VOLUME 121, NUMBER 8
MARCH 3, 1999
© Copyright 1999 by the
American Chemical Society

JOURNAL OF THE AMERICAN CHEMICAL SOCIETY

Ordering of Fractal Clusters in Crystallizing Lysozyme Solutions

Yannis Georgalis,*,† Patrick Umbach,*,†,‡ Wolfram Saenger,† Bernd Ihmels,§ and Dikeos Mario Soumpasis§

Contribution from the Institut für Kristallographie, Freie Universität Berlin, Takustrasse 6, 14195 Berlin, Germany, and Max-Planck Institut fur Biophysikalische Chemie, Biocomputation Group, Postfach 2841, 37018 Göttingen, Germany

Received July 8, 1998

Abstract: The cluster formation in nucleating hen egg white lysozyme−NaCl solutions was studied by simultaneous static and dynamic light scattering. Angular dependence measurements of the total scattered intensity and of the average cluster diffusion coefficient revealed the appearance of pronounced structure factor peaks at the initial nucleation stages. Such peaks are characteristic for the ordering often observed in highly concentrated colloidal suspensions. Free-energy minimizations of 4−60 particles, that adequately model the lysozyme monomer, were performed by using the effective interaction potentials described in previous work (Soumpasis; Georgalis *Biophys. J.* **1997**, *72*, 2770). Both experiment and computations show formation of clusters with fractal morphology, compatible with the findings of the present and previous works.

Introduction

The crystallization of proteins is a major obstacle in elucidating their three-dimensional structures at atomic resolution. Protein crystal growth is a time- and material-consuming endeavor, based on empirical "trial-and-error" recipes without reliable diagnostic tools. Considerable effort has been made in recent years to understand the mechanism underlying biomolecular crystallization and establish conditions that promote growth of crystals suitable for X-ray diffraction studies. However, due to principal difficulties in predicting and monitoring interactions at high protein and electrolyte concentrations, the development of diagnostic techniques is still lacking a rigorous physical-chemical background.

Interactions between particles in solution can be probed by small-angle X-ray or neutron scattering techniques.[1] If the particles are large enough, one can use the spatiotemporal scales covered by conventional static (SLS) and dynamic (DLS) light scattering techniques[2,3] to examine interparticle interactions (for a review on this issues see ref 4). Several prominent events associated with the nucleation and crystallization of colloids have been unravelled by light scattering.[5,6] Details on the dynamics of nucleation and growth have been obtained by time-resolved SLS and DLS or small-angle SLS studies.[7−17]

* To whom correspondence should be addressed. Tel: ++04930-838-4588. Fax: ++04930-838-6702. E-mail: yannis@chemie.fu-berlin.de.
† Freie Universität Berlin.
‡ Current address: Abbott Laboratories, Dept. of Structural Biology, Optical Spectroscopy Laboratory, Abbott Park, IL.
§ Max-Planck Institute für Biophysikalische Chemie.

(1) Ottewill, R. H. *Langmuir* **1989**, *5*, 4.
(2) Berne, B.; Pecora, R. *Dynamic Light Scattering*; Academic Press: New York, 1974.
(3) Brown, W. *Dynamic Light Scattering, the Method and Some Applications*; Ed., Oxford Science Publications: Oxford, 1993.
(4) Pusey, P. N.; Tough, R. J. A. In *Dynamic Light Scattering*; Pecorra, R., Ed.; Plenum Press: New York, 1985; p 85.
(5) Pusey, P. N. In *Liquids, Freezing and Glass Transition*; Hansen, J. P., Levesque, D., Zinn-Justin, J., Eds.; Elsevier: Amsterdam, 1991; p 765.
(6) Poon, W. C. K.; Pusey, P. N. In *Complex Fluids*; Baus, M., et al., Eds.; Kluwer: Netherlands, 1995; p 3.
(7) Pusey, P. N. In *Neutron, X-Ray and Light Scattering*; Lindner, P., Zemb, Th., Eds.; North-Holland: Amsterdam, 1991.
(8) van Megen, W.; Pusey, P. N. *Phys. Rev. A.* **1991**, *43* (10), 5429.
(9) Dhont, J. K. G.; Smits, C.; Lekkerkerker, H. N. W. *J. Colloid Interface Sci.* **1992**, *152* (2), 386.
(10) van Megen, W.; Underwood, S. M. *Nature* **1993**, *362*, 616.

10.1021/ja982407y CCC: $18.00 © 1999 American Chemical Society
Published on Web 02/13/1999

In contrast to those on colloids, investigations on protein crystallization are still sparse (for a review see ref 18). The direct extrapolation of nucleation events from collloids to proteins is, however, not straightforward. Typical colloids used in nucleation studies are uncharged and interact primarily through excluded volumn effects and crystallize nearly homogeneously at high volume fractions. In contrast, charged proteins crystallize heterogeneously, at much lower volume fractions, when their charges are screened using suitable electrolytes, at rather high concentrations. Crystallization may also be induced at lower electrolyte concentrations, in the presence of concentrated inert polymers such as polyethylene glycols or dextrans.

Numerous experimental studies using small-angle neutron or X-ray scattering on ionic micelles[19] and on hydrophilic proteins in aqeous solutions[20] have identified pronounced peaks in the distribution of the scattered intensities. The peaks are localized at finite scattering vectors |q| approximately equal to 2π times the reciprocal of the mean interparticle separation distance. The effective interactions involved in such systems depend primarily on the characteristics of the protein (charge and size) as well as on the characteristics of the added electrolyte[21] (size, valency, etc.). Knowledge of these parameters is important for the computation of thermodynamic and transport properties of solutions. Theoretically, the study of correlations in charged protein solutions may be accomplished via routes analogous to those applied in mixed electrolyte or molten salt systems. However, there is a fundamental difference between them: The size and charge of proteins are usually much larger than those of the salt ions. Therefore, proteins are considered asymmetric electrolytes. The high protein charge leads to a "pileup" of counterions on the protein surface, and their net charge, as determined by scattering techniques, appears to be lower than that determined by potentiometric titrations. Since protein−counterion correlations are intimately coupled to protein−protein correlations through the Ornstein−Zernike (OZ) equation,[22] poor approximations in evaluating the protein−counterion correlations unavoidably affect the accuracy of the protein−protein potential of the mean force (PMF) calculations. Sophisticated theoretical and computational treatments are therefore necessary to quantitatively determine the prevalent effective interactions involved in the computations of PMFs.[23,24]

We have shown in previous works that descriptions of the aggregation events, even with a simple system such as lysozyme−NaCl, are not easy. One major problem is that the temporal scales typifying the diffusive motion of small globular proteins are quite short, and therefore, high-speed techniques are required to capture the underlying events. Kinetic results on supersaturated lysozyme solutions are limited so far to time-resolved DLS experiments performed at fixed forward scattering angles[25−30] or time-resolved small-angle SLS.[31] [In complex protein−electrolyte solutions it is not correct to use the supersaturation in its classical definition, due to the large number of species involved. Further, supersaturation is a quantity that is defined at equilibrium. We use the term "supersaturation" only as a convenient abbreviation for identifying different protein and electrolyte concentration combinations.] Such experiments are best performed at moderate supersaturation levels to avoid the development of multiple light scattering.

For the studies described here, we have employed the system lysozyme−NaCl in an aqueous buffered solution and modified the solution supersaturation by varying the temperature and protein and/or electrolyte concentration. By using an improved detection system, we can detect up to three individual populations in nucleating lysozyme solutions. The first is attributed to lysozyme monomers or oligomers, the second to nuclei, and the third to fractal clusters formed from collisions between nuclei immediately upon addition of electrolyte. The monomers (or oligomers) are small but present at very large amounts in solution. In contrast, fractals are very few but large and dominate scattering, especially at forward scattering angles. Nuclei are larger than monomers and oligomers, but they are present only in limited amounts. Most of them collapse and form large fractal clusters; only few survive and promote growth of macroscopic crystals.

Fractal Growth

In typical growth experiments, small clusters recombine to form larger ones, and the process repeats itself at larger scales until all the available material is exhausted or the clusters are unable to move (gel formation). If no restructuring occurs during growth, the final cluster is made of clusters produced at earlier growth stages similar to each other, and the resulting structures are termed fractals.[32,33] The observation of the final object on short scales reveals the structure of clusters produced in the early stages, whereas the organization at larger scales reveals properties of late growth structures. If the same growth process repeats itself at every scale, the resulting structure is the same at every scale and is termed self-similar.

A self-similar mass-fractal is defined[34,35] as an object for which the minimum number of cubes of edge L, needed to cover it, scales as $N(L) \propto L^{-d_f}$, with $d_f < 3$ denoting its mass-fractal dimension. This scaling law is valid between two characteristic cutoff lengths limited by the monomer size and the radius of

(11) van Megen, W.; Underwood, S. M. *Phys. Rev. Lett.* **1993**, *70* (18), 2766.
(12) van Megen, W.; Underwood, S. M. *Phys. Rev. E* **1994**, *49* (5), 4206.
(13) Schätzel, K.; Ackerson, B. J. *Phys. Rev. Lett.* **1992**, *68* (3), 337.
(14) Schätzel, K.; Ackerson. B. J. *Phys. Rev. Lett.* **1993**, *48* (5), 3766.
(15) Ackerson, B. J.; Schätzel, K. *Phys. Rev. E* **1995**, *52* (5), 6648.
(16) Harland, J. L.; Henderson, S. I.; Underwood, S. M.; van Megen, W. *Phys. Rev. Lett.* **1995**, *75* (19), 3572.
(17) He, Y.; Ackerson, B. J.; van Megen, W.; Underwood, S. M.; Schätzel, K. *Phys. Rev. E* **1996**, *54* (5), 5286.
(18) Giegé, R.; Drenth, J.; Ducruix, A.; McPherson, A.; Saenger, W. *Prog. Cryst. Growth Charact.* **1995**, *30*, 237.
(19) Chen, S.-H. *Annu. Rev. Phys. Chem.* **1986**, *37*, 351.
(20) Chen, S.-H.; Bendedouch, D. In *Methods in Enzymology*; Hirs, C. H., Timashef, S. N., Eds.; Academic Press: New York, 1986.
(21) Verwey, E. J.; Overbeek, J. Th. G. *Theory of the Stability of Lyophobic Colloids*; Elsevier: New York, 1948.
(22) Hansen, J. P.; McDonald, I. R. *Theory of Simple Liquids*; Academic Press: New York, 1986.
(23) Soumpasis, D. M. In *Computations of Biomolecular Structures*; Soumpasis, D. M., Jovin, T., Eds.; Springer Verlag: Berlin, 1993; p 223.
(24) Soumpasis, D. M.; Georgalis, Y. *Biophys. J.* **1997**, *72*, 2770.
(25) Georgalis, Y.; Zouni, A.; Eberstein, W.; Saenger, W. J. *Cryst. Growth* **1993**, *126*, 245.
(26) Georgalis, Y.; Saenger, W. *Adv. Colloid Interface Sci.* **1993**, *46*, 165.
(27) Georgalis, Y.; Schuler, J.; Frank, J.; Soumpasis, D. M.; Saenger, W. *Adv. Colloid Interface Sci.* **1995**, *58*, 57.
(28) Tanaka, S.; Yamamoto, M.; Kawashima, K.; Ito, K.; Hayagawa, R.; Ataka, M. *J. Cryst. Growth* **1996**, *168*, 44.
(29) Georgalis, Y.; Umbach, P.; Raptis, J.; Saenger, W. *Acta Crystallogr. D* **1997**, *53*, 691.
(30) Georgalis, Y.; Umbach, P.; Raptis, J.; Saenger, W. *Acta Crystallogr. D* **1997**, *53*, 703.
(31) Umbach, P.; Georgalis, Y.; Saenger, W. *J. Am. Chem. Soc.* **1998**, *120* (10), 2382.
(32) Meakin, P. In *Phase Transitions and Critical Phenomena*; Domb, C., Lebowitz, L. L., Eds.; Academic Press: New York, 1988; Vol. 12, p 351.
(33) Kolb, M. In *Large-Scale Molecular Systems*; Gans, W., Blumen, A., Aman, A., Eds.; Plenum Press: New York, 1991; p 231.
(34) Teixeiera, J. In *On Growth and Form*; Stanley, E. H., Ostrowsky, N., Eds.; M. Nijhoff: Boston, 1986; p 145.
(35) Sinha, S. K. *Physica D* **1989**, *38*, 310.

gyration, R_g^C, which describes the physical size of a fractal cluster. The mass-fractal dimension is not an integer, $d_f = 3$ being the limiting case of an Euclidian body. Therefore, for mass-fractals with $d_f < 3$, a larger radius of gyration indicates lower density or formation of tenuous clusters. These laws are valid if growth propagates over many length scales. In aggregation of small colloids the shortest scale is the seeding particle radius and the largest scale corresponds to the upper limit of Brownian motion, i.e., a few μm. Above this latter scale, gravity and hydrodynamic flow of the solvent become dominant[36,37] and the fractals collapse by their own weight and sediment.

Light Scattering

For a better understanding of the experimental results, it is necessary to provide a brief summary of the theory involved in this analysis. In scattering experiments the spatial resolution is defined by the scattering vector q, whose magnified is given by the Bragg condition

$$q = \frac{4\pi n}{\lambda}\sin\left(\frac{\theta}{2}\right) \tag{1}$$

where λ denotes the wavelength of the light, n is the refractive index of the solution, and θ is the scattering angle. The vectors of the incident and scattered light define virtual fringe planes with spacing $L = \pi/q$, and particles aligned along these planes scatter light in the direction of the observation angle θ.

Static light scattering (SLS) accesses the equilibrium structure in terms of the product of the single-particle form factor $P(q)$ and static structure factor $S(q)$. Dynamic light scattering (DLS) provides information on particle diffusive motion through the dynamic structure factor,[5] $F(q, \tau)$. Both techniques yield results statistically averaged over a large ensemble of particles contained in the scattering volume.

Static Light Scattering (SLS). The basis for analyzing concentration fluctuations is the pair correlation function $g(r)$.[22] The inverse Fourier-transform of $g(r)$ delivers the static structure factor $S(q)$, which is the quantity measured in most scattering experiments:

$$S(q) = 1 + 4\pi\bar{c}\int_0^\infty r^2[g(r) - 1]\frac{\sin(qr)}{qr}\,dr \tag{2}$$

$\bar{c} = N_0/V$ denotes the concentration of seeding particles in the scattering volume V for a given scattering vector q, and r is the distance between two particles.

Th spatial distribution of the interacting particles can be studied by measuring the angular dependence of the total scattered intensity $I(q)$. The latter is expressed as the product of the static structure factor, $S(q)$, and the particle form factor, $P(q)$, which depends only on the shape of the considered particles, but not on the interactions between them. Usually, $P(q)$ can be determined from dilute solutions, if the particle radius α compares with the wavelength. For spherical scatterers with a radius α,[2]

$$P(q) = \left\{\frac{3}{(q\alpha)^3}[\sin(q\alpha) - q\alpha\cos(q\alpha)]\right\}^2 \tag{3}$$

We can then write $I(q)$ as

$$I(q) \propto \bar{c}S(q)P(q) \tag{4}$$

Equation 4 is equivalent to the ratio of the total scattered intensity of an interacting solution to that of a similar but noninteracting solution at the same q. At small scattering angles, $P(q) \simeq 1$, and therefore, $I(0) \propto S(0)$.

Dynamic Light Scattering (DLS). DLS can access the time scales during which scattered light intensity fluctuations decay. If the fluctuations are solely due to Brownian motion of the particles, the intensity autocorrelation function (ACF) decays as a single expotential with a rate $2D(q)q^2$, where $D(q)$ denotes a, q-dependent, diffusion coefficient.

For monodisperse, noninteracting particles one determines a "dynamic structure factor", $F(q, \tau)$, given by a single-exponential decay as[4]

$$F(q, \tau) = \exp(-2q^2D_0\tau) \tag{5}$$

where D_0 denotes the "free-particle" diffusion coefficient.

At moderate to high concentrations, $F(q, \tau)$ deviates from the single-exponential decay with time, and a higher order cumulant expansion[38] of the form

$$\ln[F(q, \tau)] = -\kappa_1(q)\tau + \frac{1}{2!}\kappa_2(q)\tau^2 - \frac{1}{3!}\kappa_3(q)\tau^3 + O(\tau^4) \tag{6}$$

is used to approximate the ACF.

In eq 6, $\kappa_i(q)$ denotes the ith cumulant of the ACF determined at a scattering vector q. Of interest is the first cumulant:

$$\kappa_1(q) = 2D_0(q)q^2 \tag{7}$$

which typifies the time decay of $F(q, \tau)$ for $\tau \rightarrow 0$. The diffusion coefficient determined in a classical boundary diffusion experiment corresponds to $D(q = 0)$. If the solution is sufficiently dilute and the particles small compared to the wavelength, D does not depend on the scattering vector q, and the Stokes–Einstein relation can be employed to deduce the hydrodynamic radius a, assuming spherical particles moving in a solvent with viscosity η:

$$D = \frac{k_BT}{6\pi\eta\alpha} \tag{8}$$

If particle interactions are significant, the trajectories of different particles are correlated. No general theory is yet available to predict the full dependence of this correlation on delay time τ and the scattering vector q.[39]

For monodisperse systems the dynamic structure factor can be expressed as

$$F(q, \tau) = \frac{S(q, \tau)}{S(q, 0)} \tag{9}$$

where $S(q, \tau)$ denotes a "measured static structure factor". Without hydrodynamic interactions, the latter is expressed as a function of D_0 and of the effective diffusion coefficient:[40]

$$D(q) = \frac{\kappa_1(q)}{q^2} = \frac{D_0}{S(q)} \tag{10}$$

Usually D_0 is determined in dilute solutions. Finally it should

(36) Lin, M. Y.; Lindsay, H. M.; Weitz, D. A.; Ball, R. C.; Klein, R.; Meakin, P. *Nature* **1989**, *339*, 360.
(37) Lin, M. Y.; Lindsay, H. M.; Weitz, D. A.; Ball, R. C.; Klein, R.; Meakin, P. *Proc. R. Soc. London A* **1990**, *423*, 71.
(38) Koppel, D. E. *J. Chem. Phys.* **1972**, *57*, 4814.
(39) Schätzel, K. *Adv. Colloidal Interface Sci.* **1993**, *46*, 309.
(40) Ackerson, B. J. *J. Chem. Phys.* **1976**, *64*, 242; **1978**, *69* (2), 684.

be mentioned that structure factors deduced by SLS or DLS should ideally coincide. [The determination of $S(q)$ by DLS has the advantage that neither absolute intensities nor form factor corrections are required.]

Materials and Methods

The chemicals used in the present work were of analytical grade. Lysozyme was purchased from Sigma Chemicals (Deisenhofen, Germany) and treated as previously described.[29] All experiments were conducted in a buffer containing 0.10 M Na−acetate, pH 4.25. NaCl, p.a. grade, was from Merck (Darmstadt, Germany). Monodispersity of the preparations was controlled by DLS in experiments without added electrolyte. For aggregation experiments, lysozyme and NaCl were prepared as stock solutions in this buffer, rapidly mixed in the appropriate ratio and filtered (Minisart sterile filters, 0.2 μm pore size) into cylindrical quartz cells. Monitoring of the reaction was initiated within less than 30 s after mixing lysozyme and NaCl solutions.

Light Scattering. Light scattering measurements were performed with an ALV/SP−86 apparatus equipped with ALV-FAST/5000E digital autocorrelators. A tunable Ar^+ laser (Specrtaphysics, 2017) operating at a wavelength of 488 nm was employed in these studies. Scattering was monitored using an ALV/SO-SIPD detector unit mounted on a goniometer arm, and the angular range between 15° and 150° was covered with a resolution of 2.5°. A second ALV/SO-SIPD detector unit, fixed at a scattering angle of 270° (90°), served for monitoring the events as a function of time. A fraction of the incoming beam was monitored continuously by two quadrant photodiodes placed after a precision attenuator. The readings of the photodiodes were employed to normalize the total scattered intensities and to exclude artifacts stemming from long-term fluctuations or changes in the pointing stability of the beam.

The correlator was most often operated in the dual mode; that is, two different data sets were simultaneously obtained during each experiment. The first set involved SLS and DLS records acquired at each angle, and the second time-resolved data collected with the fixed detector. Practically no differences are found if these experiments are performed with the first detector operating in (pseudo)-cross-correlation mode while using a second correlator to acquire the data at 90°. Scattered light intensities at forward scatterign angles (i.e. 15−20°) exceed by several times those detected at 90°. Therefore, when using both detectors, care should be exercised to have signals strong enough for the fixed detector, while not violating the linearity of the scanning photomultiplier. Typical ACFs, both as a function of the scattering vector q and at the fixed scattering angle of 90°, are displayed in Figure 1. The spectra indicate the existence of polymodal distributions where contributions from fractal clusters are pronounced due to the intensity preserved weighting contributions on the ACF.

In previous works we have used the Laplace inversion algorithm CONTIN[41] for decoupling the various species involved. In this work we have performed the data reduction with the simpler method of cumulants[38] utilizing only the first 32−128 μs of the ACF, depending on angle. This method delivers only a weighted average of the effective diffusion coefficient D that typifies only the smallest species prevailing in solution, i.e., those corresponding to oligomers and probably nuclei. The contributions from the larger fractal clusters are implicitly neglected. However, the coincidence with the SLS experiment, which measures the same average contributions, indicates that most of the scattering events can be attributed to these smaller species. The values obtained for $D(q)$ should be understood as those closely matching the respective SLS scans. Estimates for $D(q)$ and $D(90°)$ are lower by 5−15 times than those typifying the diffusion coefficient of the monomeric lysozyme ($D_0 = 10.6 \times 10^{-7}$ cm^2 s^{-1}, $\alpha = 1.96$ nm[42]) in this buffer.

Deduction of the Peak Characteristics. We have employed the estimates of scattered intensity, $I(90°)$, and of the diffusion coefficient, $D(90°)$, to normalize $I(q)$ and $D(q)$, collected at each angle, and determine an "apparent structure factor" $S_{app}(q)$, defined as

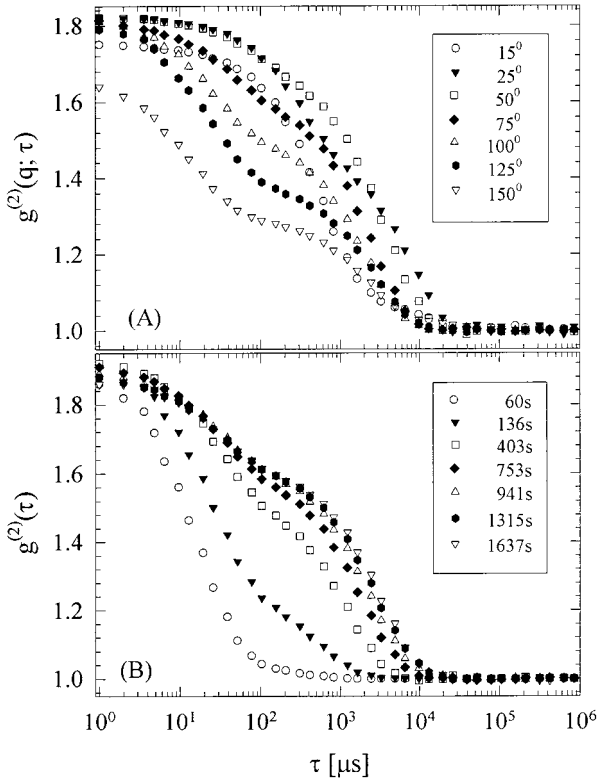

Figure 1. ACFs from (A) a selected angular scan; the respective angles are given in the inset. (B) Simultaneous detection at 270° (90°); the corresponding times are given in the inset. For this particular experiment, 2.1 mM lyzozyme was incubated with 0.60 M NaCl at 293.2 K in Na−acetate buffer, pH 4.25. For the sake of clarity only every fourth channel of each ACF is displayed.

$$S_{app}(q) = \frac{I(q)}{I(90°)}$$

$$S_{app}(q) = \frac{D(90°)}{D(q)} \qquad (11)$$

This operation is not absolutely correct since it introduces an artificial normalization of the peak amplitude to unity at scattering vectors corresponding to 90°. Further, the rapid cluster growth and the spatial resolution required allow one to observe only a single structure factor peak with confidence, and further time-resolved information is lost. At later times, i.e., in the second and third scan, the peak escapes observation and a power-law decay, typical for fractal cluster formation, is observed (when the respective DLS or SLS data are plotted in doubly logarithmic scales).

We illustrate these operations in Figure 2, panels A−D. In panels A we have plotted the raw angular data $D(q)$ vs q and in B those collected at 90°, $D(90°)$ vs t. Note that in B two different slopes, with values of 0.74 and 0.41, can be deduced from these kinetics, when the data are plotted in a doubly logarithmic scale. However, we do not believe that angles as high as 90° deliver adequate estimates of the exponents typifying aggregation. We, therefore, use these data only for normalization purposes. In panel C we have plotted $D_0/D(q)$ vs q using for D_0 the diffusion coefficient corresponding to monomeric lysozyme. This resembles the equivalent treatment for a stationary concentrated suspension. In panel D we have plotted $D(90°)/D(q)$ vs q using the respective 90° data shown in panel B. Whereas drastic changes in the peak shape and amplitude are evident when comparing panels C and D, the peak location changes only very little. The SLS records exhibit similar behavior when similarly treated, but they are considered more reliable since they are not subjected to any fitting manipulations.

Quantitative estimates of peaks originating from a process like spinodal decomposition can be deduced by invoking the structure factors

(41) Provencher, S. W. *Comput. Phys. Commun.* **1982**, *27*, 213; **1982**, *27*, 229.

(42) Eberstein, W.; Georgalis, Y.; Saenger, W. *J. Cryst. Growth* **1994**, *143*, 71.

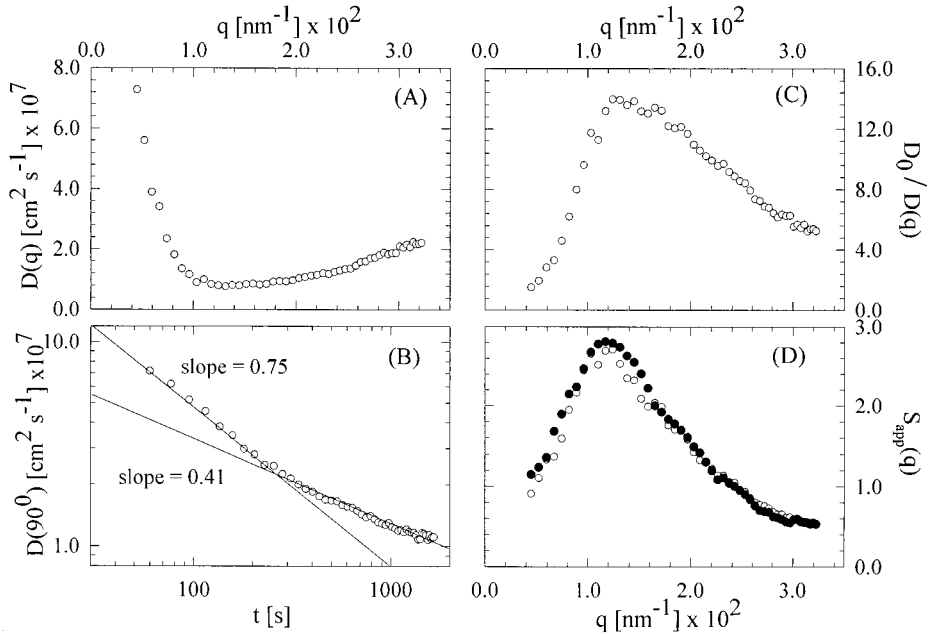

Figure 2. Peak deduction from the experiment in Figure 1. (A) Dependence of the apparent cluster diffusion coefficient $D(q)$ as a function of the scattering vector q. (B) Apparent diffusion coefficient $D(90°)$, as a function of the reaction time t. Note the biphasic character of the plot with time. In (C) is plotted $D_0/D(q)$ vs q using for D_0 the diffusion coefficient of the lysozyme monomer. In panel (D) we have employed the time-resolved data from (B) to "normalize" $D(q)$ from (A) and obtain $D(90°)/D(q)$ vs q. Closed symbols indicate typical comparison of the peak from the respective SLS scan. Note the agreement between SLS and DLS records (for details see text).

theoretically developed by Furukawa[43] or those employed by Schätzel and Ackerson[13,14] for nucleation and growth. As shown in a recent small-angle SLS study,[44] these expressions can describe satisfactorily the events.

In this study we have employed the structure factor of Hashimoto et al.,[45] which reads

$$S(Q) = \frac{S(q)}{S_m} = \frac{Q^2}{\gamma/2 + Q^{2+\gamma}} \quad \text{with} \quad Q = \left(\frac{q}{q_m}\right) \qquad (12)$$

In the analyses, the scattering amplitude S_m and the scattering vector q_m, which typify the peak properties at the maximum, and the exponent γ were treated as fitting parameters. Estimates of q_m are used to define a mean radius, R, of the evolving domains, whereas γ provides insights on the cluster morphology. The exponent γ is associated with the cluster fractal dimension as follows: $\gamma = 2d_f$ for critical and $\gamma = d_f + 1$ for off-critical mixtures.[45] This phenomenological description provides useful insights in the behavior of the system, particularly when more rigorous theories are unavailable.

It should be mentioned that the examined conditions are distant to known critical conditions for the system lysozyme−NaCl.[46−50] If the system is close to the critical point, nucleation rates are very fast, clusters grow very rapidly, and the structure factor peaks of the lysozyme−NaCl system can be detected only at small scattering angles.[44] Away from critical points, ordering is still expected to be observed; however, clusters are expected to be initially smaller, and thus ordering can be easier captured by light scattering at conventional scattering angles. This latter case is examined in the present work.

Computations on Cluster Formation. In a recent computational work[24] we have shown that the effective interaction PMFs between lysozyme monomers, which govern aggregation and concomitant crystallization, depend in complex ways on thermodynamic state parameters (e.g., protein and electrolyte concentration, size, charge). Due to the slow kinetics underlying aggregation and cluster formation in the examined systems, in principal straightforward dynamic simulations, using these PMFs, are technically not feasible in order to obtain quantitative estimates of cluster morphology, size, and stabilities. To accomplish this task, we here use minimization of the PMF-free energies in small lysozyme clusters comprising 4−60 monomers, at electrolyte concentrations found to either favor or preclude significant aggregation and subsequent crystallization.

In previous work on electrolytes[51,52] we have found that the Kirkwood approximation[53] is adequate in systems with spherically symmetric pair interactions up to rather high concentrations. The PMFs obtained via solution of the hypernetted chain (HNC) equation[54,55] were accurately parametrized via spline functions.

The computations proceed as follows: We generate random initial configurations of the 4−60 spheres modeling lysozyme molecules interacting via the PMFs corresponding to the conditions chosen (i.e., electrolyte and protein concentration). We then minimize the total free energy, approximated by the sum of the pairwise PMF interactions (Kirkwood superposition principle), using standard Newton−Raphson optimization. We then obtain representative clusters after repeating this process, initial configuration−minimized configuration, several thousand times (up to 6×10^3), depending on cluster size.

Results

The optimal lysozyme and NaCl concentrations for crystallization are around 1.5 mM and 0.60 M, respectively[27−30] at 293.2 K. Under these conditions, crystals grow within less than two days as judged by optical microscopy. Therefore, conditions were chosen below, at and above these concentrations of

(43) Furukawa, H. *Physica A* **1984**, *123*, 497.
(44) Georgalis, Y.; Umbach, P.; Soumpasis, D. M.; Saenger, W. *J. Am. Chem. Soc.* **1998**, *120* (22), 5539.
(45) Hashimoto, T.; Itakura, M.; Hasegawa, H. *J. Chem. Phys.* **1985**, *85* (10), 6118.
(46) Ishimoto, C.; Tanaka, T. *Phys. Rev. Lett.* **1997**, *39*, 474.
(47) Phillies, G. D. J. *Phys. Rev. Lett.* **1985**, *55*, 1341.
(48) Taratuta, V. G.; Holschbach, A.; Thurston, G. M.; Blankschtein, D.; Benedek, G. B. *J. Phys. Chem.* **1990**, *94*, 2140.
(49) Broide, M. L.; Tominc, T. M.; Saxowsky, M. *Phys. Rev. E* **1996**, *53*, 6325.
(50) Muschol, M.; Rosenberger, F. *J. Chem. Phys.* **1997**, *107* (6), 1953.
(51) Hummer, G.; Soumpasis, D. M. *Mol. Phys.* **1992**, *75*, 633.
(52) Hummer, G.; Soumpasis, D. M. *J. Chem. Phys.* **1993**, *98*, 581.
(53) Kirkwood, J. G. *J. Chem. Phys.* **1935**, *3*, 300.
(54) Van Leewen, J. M. J.; Groeneweld, J.; De Bower, J. *Physica* **1959**, *25*, 792.
(55) Morita, T.; Hiroike, K. *Progr. Theor. Phys.* **1961**, *25*, 537.

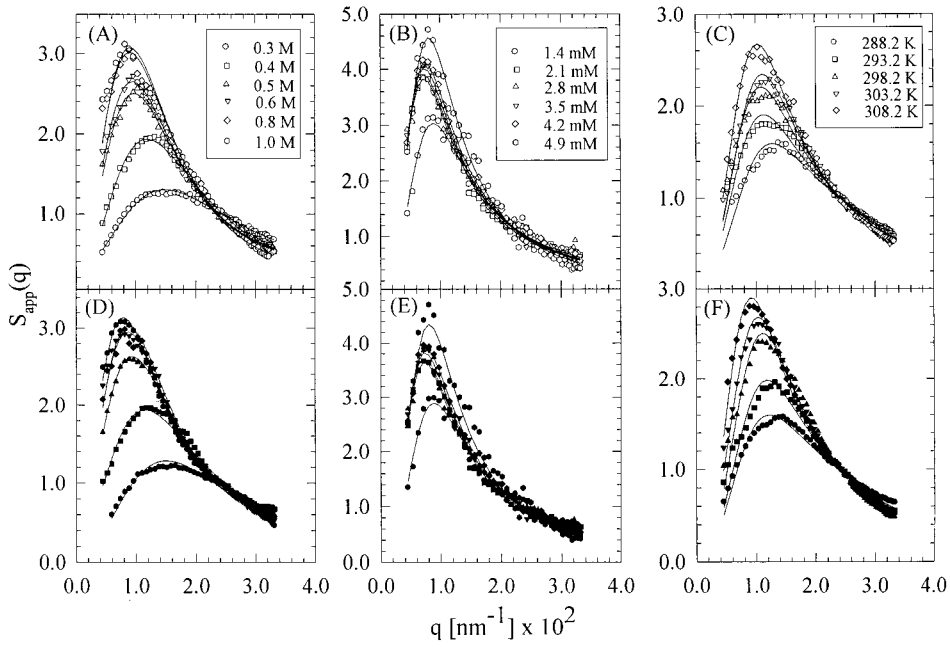

Figure 3. Structure factor peaks of nucleating lysozyme solutions determined by simultaneous DLS (upper panels, open symbols) and SLS (lower panels, closed symbols). In (A) and (D) lysozyme concentration was 2.1 mM and NaCl was varied between 0.3 and 1.0 M (individual concentrations are given in the inset). In (B) and (E) NaCl concentration was 0.60 mM and lysozyme concentration was varied between 1.4 and 4.9 mM (individual concentrations are given in the inset). In (C) and (F) lysozyme was 2.1 mM and NaCl 0.6 M. The reaction temperature was varied between 288.2 and 308.2 K with steps of 5.0 K (individual temperatures are given in the inset). All measurements were conducted in Na−acetate buffer pH 4.25. Note that in all cases the maximum peak position moves to smaller scattering vectors with increasing NaCl and lysozyme concentration or temperature, indicating formation of larger clusters. The fits through the data correspond to eq 12; typical results are given in Figure 4.

lysozyme and NaCl. The range of temperature variation was taken from a previous work.[56]

In the first set of experiments we have followed the peak development using a constant lysozyme concentration, 2.1 mM, and varying the NaCl concentration between at 0.30 and 1.0 M. Six experiments were conducted in a buffer containing 0.10 M Na−acetate, pH 4.25, at 293.2 K, Figure 3A, D. In the second set of experiments, the peak development was followed as a function of lysozyme concentration at a constsant NaCl concentration, 0.60 M. The concentration of lysozyme was varied between 1.39 and 4.89 mM. Six experiments were conducted in a buffer containing 0.10 M Na−acetate, pH 4.25, at 293.2 K, Figure 3B,E. In the third set of experiments we varied the solution temperature from 283.2 to 303.2 K, and the events were followed at a constant NaCl, 0.60 M, and lysozyme, 0.21 mM, concentration. These data are shown in Figure 3C,F.

In all these 17 experiments, the peaks migrate to smaller scattering vectors as a function of solution supersaturation. The respective mean cluster radius R and estimates of the exponent g are obtained from nonlinear fits to the normalized data of Figure 3. The estimates of R and γ are shown in Figure 4 as a function of salt and protein concentration and temperature. Both of them exhibit extrema at around 0.8 M NaCl and 3.2 mM lysozyme. In contrast, a linear behavior on temperature is observed.[56] In comparison to previous works, the extrema shown in the first two cases appear at somewhat higher concentrations of NaCl and lysozyme. This behavior can be explained if one considers that here only gross average quantities are measured. The values of the exponent γ are unexpected, since they seem to resemble closely d_f but not $2d_f$ or $d_f + 1$. This has been pointed out also in a study by He et al.,[17] when using a volume fraction dependent γ and a modified Furukawa structure factor. The authors have attributed qualitative significance to this variable. Analyses of the results shown in Figure 3 with the He et al. structure factors delivered exponents, γ, were nearly identical to those quoted in Figure 4D−F.

Finally, we have examined three lysozyme concentrations 0.71, 2.1, and 3.5 mM incubated with 0.30, 0.60, and 0.90 M NaCl each. The structure factors derived from these experiments were very similar to those depicted in Figure 3 (data not shown). They were easily detectable with 0.60 and 0.90 M NaCl, but it was not possible to conclude about structure formation in experiments conducted with 0.30 M NaCl. In this salt concentration clusters were formed only sparingly and the peaks could not be determined with confidence. The results from these experiments will be treated in detail in a subsequent communication.

Despite the unavoidable normalization of the angular data with those obtained with the detector at 90°, the agreement between the estimates obtained by SLS and DLS is reasonable. Differences observed between equivalent data sets are attributed to the different lysozyme preparations and instrumental adjustments. Operations like mixing and filtering, which are performed manually, also give rise to small but measurable differences.

Another point that should be addressed in these studies is the development of multiple scattering, which prohibits the study of higher protein−electrolyte concentrations. Unfortunately, isorefractive conditions, often employed in studies of colloidal crystallization, cannot be used in nucleating protein systems. Since we cannot directly monitor the solution turbidity with our spectrogoniometer, we have repeated the experiments at the highest protein−NaCl concentrations using our small-angle SLS apparatus with transmission detection.[57] Considerable turbidity was observed only after several hours. We have also reexamined the same solutions for multiple scattering using the two-color

(56) Eberstein, W.; Georgalis, Y.; Saenger, W. *Eur. Biophys. J.* **1993**, *22*, 359.

(57) Georgalis, Y.; Umbach, P.; Zielenkiewicz, A.; Utzig, E.; Zielenkiewicz, W.; Zielenkiewicz, P.; Saenger, W. *J. Am. Chem. Soc.* **1997**, *119*, 11959.

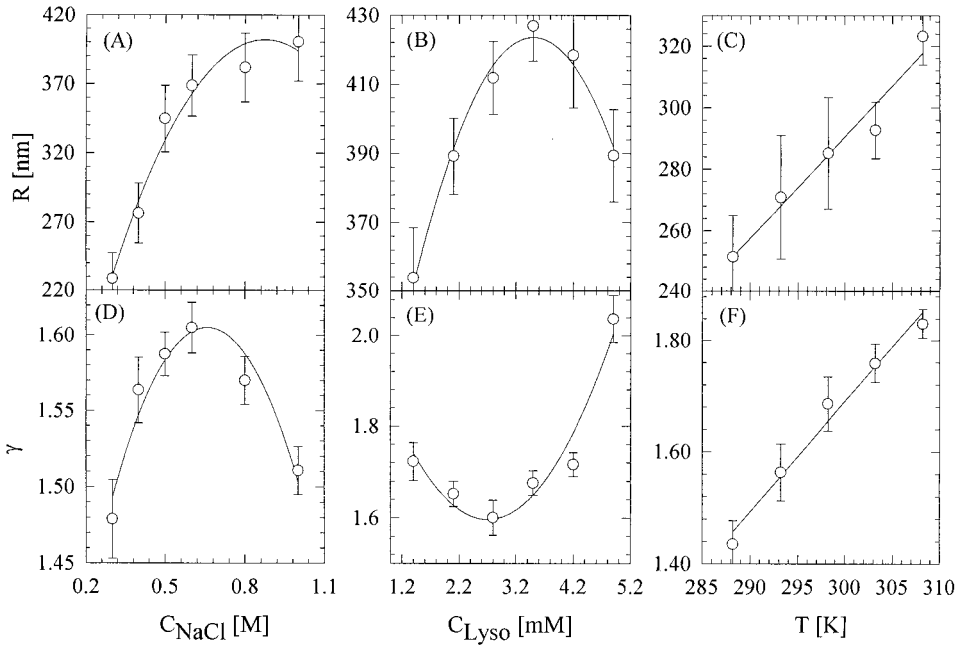

Figure 4. (Upper panels A, B, and C) Plots of the distance of the typical mean radius, *R*, obtained from the fits in the data shown in Figure 3, employing eq 12. Estimates of *R* and γ are given as averages of DLS and SLS experiments. *R* varies between 220 and 400 nm as a function of solution supersaturation. (Lower panels D, E, and F) Plots of the exponent γ for the same set of experiments. The average cluster dimensionalities vary between 1.50 and 2.0 as a function of solution supersaturation. The lines through the points serve as guides to the eye.

DLS facility[58−60] available in the University of Edinburgh, in Prof. Pusey's laboratory, and reached the same conclusion: At the supersaturation examined, the solutions do not suffer from multiple scattering contributions.

It should be stressed that goniometric devices which acquire the data sequentially have a severe speed handicap. Available multidetector setups are designed for polymer analysis and mostly stationary solutions and therefore do not provide sufficient angular resolution. One could argue that the same information could be deduced from small-angle SLS observations.[61] However, DLS is invaluable in deducing information on polymodality and solution polydispersity. Especially if hydrodynamic interactions among clusters are examined, a combination of both SLS and DLS is required. Ideally, SLS and DLS should be acquired simultaneously over a wide spatiotemporal range with a high angular resolution. It is not known to us if such an instrument exists at all. The simultaneous detection at 270° may be compensated by conducting an additional time-resolved experiment at this fixed angle, using the same stock solutions. However, due to the stochastic nature of aggregations, irreproducibilities stemming from mixing and filtering were often observed.

Finally we should mention that computations on the structure factors typifiying concentrated diffusion-limited (DLCA) clusters have been performed by Sintes et al.[62] and Sciortino et al.[63] Their results indicate that the computed structure factors scale in a way similar to that shown experimentally by Carpineti and Giglio.[64,65] Similar computations by Haw et al.[66−68] suggested that low-bonding energy between clusters may lead to coarsening with nearly compact domains and pronounced structure factor peaks, similar to those appearing in spinodal decomposition. In these computational studies, cluster polydispersity was shown to exert marked effects on the resulting final structure.

Discussion

Among first-order phase transitions, crystallization and melting processes have a long and respectable prehistory of research. The factors tuning the kinetic barriers to crystallization are the supersaturation of the liquid phase and the surface energy between liquid and crystalline phases. Close to critical points their coordinated action gives rise to high nucleation rates and formation of a large number of microcrystals. For the examined system, lysozyme−NaCl, nucleation occurs within a few minutes if the solutions are forced through the unstable region by temperature quenching.[44] In contrast, supersaturated solutions outside this regime nucleate after several hours or even days.

The experimental verification of the formation of submicroscopic domains of the nucleating phase a supersaturated solution is not easy and, in certain cases, impossible to demonstrate. Whereas nucleation lines can be theoretically computed from van der Waals temperature−density diagrams for simple systems, they cannot necessarily be measured, since a few thousand nuclei in 1 cm^3 may not be detectable at all by light scattering.[69] The situation may be even more difficult with protein solutions involving several species of variable sizes and, of course, concentrations. Due to these particular difficulties with proteins, we cannot yet claim a complete understanding

(58) Drewel, M.; Ahrens, J.; Podschus, U. *J. Opt. Soc. Am.* **1990**, *27* (2), 206.
(59) Schätzel, K. *J. Mod. Optics* **1990**, *38*, 1849.
(60) Segré, P. N.; van Megen, W.; Pusey, P. N.; Schatzel, K.; Peters, W. *J. Mod. Optics* **1995**, *42*, 1929.
(61) Schätzel, K. In *Ordering and Phase Transitions*; Arora, A. K., Tata, B. V. R., Eds.; VCH Publishers: New York, 1996; p 17.
(62) Sintes, T.; Toral, R.; Chakrabarti, A. *Phys. Rev. E* **1994**, *50*, R3330.
(63) Sciortino, F.; Belloni, A.; Tartaglia, P. *Phys. Rev. E* **1995**, *52*, 4068.
(64) Carpineti, M.; Giglio, M. *J. Phys. IV* **1993**, *3*, 39.
(65) Carpineti, M.; Giglio, M. *Phys. Rev. E* **1995**, *51*, 590.
(66) Haw, M. D.; Siwenwright, M.; Poon, W. C. K.; Pusey, P. N. *Adv. Colloid Interface Sci.* **1995**, *62*, 1.
(67) Haw, M. D.; Siwenwright, M.; Poon, W. C. K.; Pusey, P. N. *Physica A* **1995**, *217*, 231.
(68) Haw, M. D.; Poon, W. C. K.; Pusey, P. N. *Phys. Rev. E* **1997**, *56*, 1918.
(69) Goldburg, W. I. In *Light Scattering Near Phase Transitions*; Cummins, H. Z., Levanyuk, A. P., Eds.; North Holland: Amsterdam, 1983; p 531.

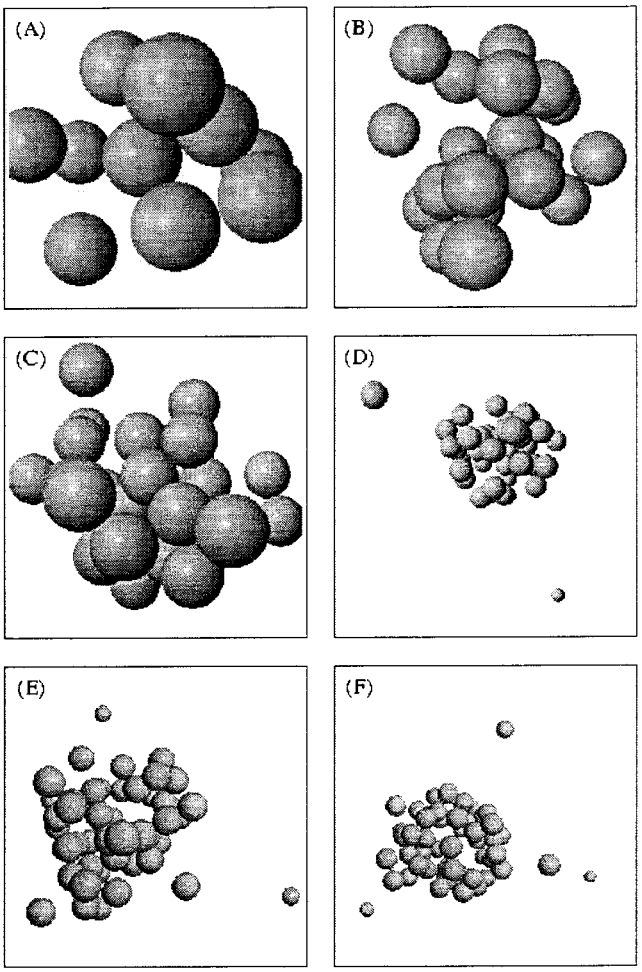

Figure 5. Typical lysozyme clusters involving 10 (panel A) to 60 (panel F) monomers. The clusters shown are those having the lowest free energy at 0.64 M NaCl at a lysozyme concentration of 2.1 mM. They were selected out of maximally 6×10^3 possible configurations using the PMFs described in ref 24.

either of the macroscopic kinetics of the transition of the underlying microscopic processes.

In this work we have observed a peak that is attributed to long-range interactions among clusters in nucleating lysozyme−NaCl solutions. The observations are, to our knowledge, made for the first time with a nucleating protein using simultaneous SLS and DLS at conventional spatiotemporal scales. The evolution of fractal clusters in nucleating lysozyme solutions could be captured so far with confidence from time-resolved DLS experiments at forward scattering angles. Results from us[27] and other investigators[28] have shown clearly the coexistence of at least two populations, identified as stationary lysozyme monomers or oligomers and larger clusters exhibiting kinetic growth. The results from this and our previous studies indicated that small nuclei, built up at the initial stages of the reaction, collide to form large fractal clusters. Using small-angle SLS,[31] isothermal microcalorimetry,[57] and scanning force microscopy,[70] we have compiled additional evidence for the appearance of clusters formed at the initial stages of the nucleation reaction. First models of the effective interparticle potentials among monomers, which are essential for qualitative insights into the problem, have been reported[24] recently. Comparisons to studies where nucleating solutions are centrifuged upon addition of the electrolyte,[71,72] thus destroying the equilibrium among the various species, are presently not possible.

The question if the structures observed in our experiments are indeed compact or fractal at the time of the peak appearance is not straightforward to answer. We have used the scaling properties of the structure factors at large q's to obtain information on this issue. In Figure 6 we have replotted selected segments of the data shown in Figure 3, in a double logarithmic scale. The ordinates are normalized with the respective amplitudes and the abscissas recast as dimensionless products, qR. In this case,[73] scaling takes place as $S(Q) \propto (qR)^{-d_f}$. A prerequisite for the validity of this expression is that $qR \gg 10$. We observe for all three cases exponents compatible with those expected for fractal growth and with those reported in Figure 4D,E,F.

Evidence corroborating the fractal morphology of the clusters, especially at the very early growth stages which cannot be monitored by light scattering can be obtained from the theoretical computations. Representative cluster populations, obtained by using the free-energy minimization procedure explained in the computational section, are shown in Figure 7. The typical minimum free-energy clusters of 4−60 lysozyme molecules exhibit fractal morphology. The observed noncompact configurations appear independent of whether conditions favor clustering or not (especially if clusters involve 10 or more monomers).

For fractal clusters consisting of N particles,[74]

$$N = \left(\frac{R_g^C}{R_g^m}\right)^{d_f} \tag{13}$$

where R_g^m is the radius of gyration of the seeding monomer.

The number of monomers N in a fractal cluster and the respective computed radius of gyration scale with an exponent $d_f = 1.77$, when plotted in a double-logarithmic scale, Figure 7. This estimate of d_f is not far from the universal pure DLCA exponent 1.81. For these computations only the minimum energy clusters at the different electrolyte concentrations were used. Slightly different values, up to 1.87, are obtained when using all data available from the free-energy minimizations.

In accordance with the cluster behavior as captured by the experiment, Figure 7, the computed clusters seem to share the same scaling property with a characteristic exponent not much different from that of pure DLCA. These findings may be used, among others, to intuitively explain why proteins crystallize at low volume fractions: Namely, the number of seeding monomers required to form a fractal nucleus of a given size is much lower than those required for a compact nucleus. Since these results do not depend on any specific details of the protein structure, we propose that they are generic.

In our opinion, effective, solvent-mediated, many-body interactions determine whether small clusters (embryos or subcritical nuclei) will form or not. If they do form, further growth and/or coalescence may take place. This in turn depends on the number density, size, and residual cluster charge of critical clusters in the immediate proximity of small clusters. Competing interactions could explain the variety of instabilities observed in nucleating lysozyme solutions (i.e., "sea-urchin" whiskers, needle- or cup-shaped microcrystals[29−31,44]). Crystal-

(70) Schaper, A.; Georgalis, Y.; Umbach, P.; Raptis, J.; Saenger, W. *J. Chem. Phys.* **1997**, *106* (20), 8587.

(71) Muschol, M.; Rosenberger, F. *J. Chem. Phys.* **1995**, *103*, 10424.

(72) Muschol, M.; Rosenberger, F. *J. Cryst. Growth* **1996**, *167*, 738.

(73) Schaefer, D. W.; Bunker, B. C.; Wilcoxn, J. P. In *Fractals in the Natural Sciences*; Fleischmann, M., Tildesley, D. J., Ball, R. C., Eds.; Princeton University Press: Princeton, NJ, 1990; p 35.

(74) Vicsek, T. *Fractal Growth Phenomena*; World Scientific: Singapore, 1989; p 81.

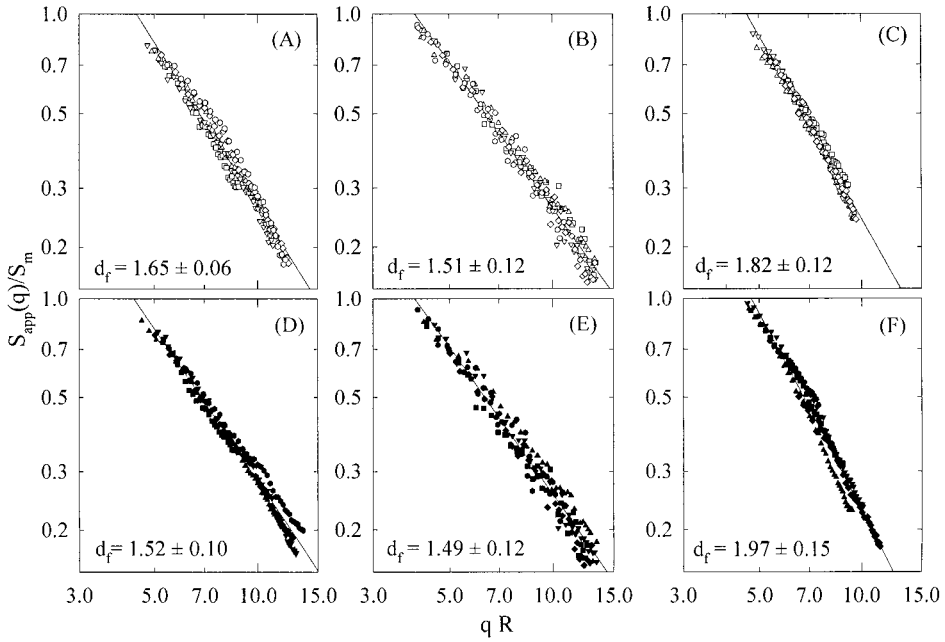

Figure 6. Scaling of the normalized data appearing in Figure 3 (see text) for details. Note that both DLS and SLS experiments collapse on master curves with slopes varying between 1.5 and 2.0, indicative of fractal cluster formation. Fractal dimensions are given individually in each panel.

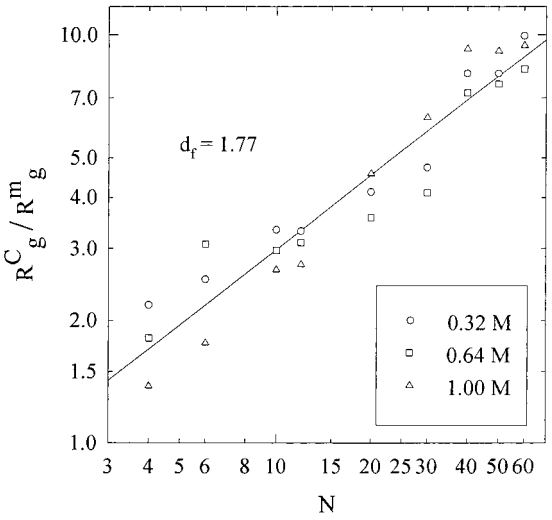

Figure 7. Scaling of the number of lysozyme monomers, *N*, involved in cluster formation as a function of the reduced cluster radius of gyration, R_g^C/R_g^m, eq 13. Minimum free-energy clusters collapse on a master curve with a mean fractal dimension $d_f = 1.77$ irrespective of the employed NaCl concentration, given the inset.

lites, i.e., finite extent clusters exhibiting the characteristic long-range order typical of macroscopic lattices, will grow only in later stages involving much larger particle numbers. These transformations may involve complex restructuing operations among the various instabilities. The symmetry and geometry of subcritical clusters do not have to resemble those of critical clusters, which is a result of restructuring. This type of behavior is shown here via PMF minimizations of solution models, but is also well-known from extensive studies of simple vacuum clusters.[75,76] The symmetry of those clusters is often related to icosahedra,[77] completely unlike crystals gorwn via coalescence, where icosahedral symmetry is forbidden.

We conclude that the structure factor peaks result from the interplay between packing and electrostatics which gives rise to long-range ordering. Both $I(q)$ and $D(q)$ are significantly modified during the early stages of the nucleation reaction, and the observed peaks may allow for a rapid first-order screening of supersaturated solutions. Although their appearance does not guarantee growth of crystals suitable for X-ray diffraction, we propose that our approach can be employed to exclude unsuitable crystal growth conditions, already at the very early stages of screening attempts.

Acknowledgment. This work was supported by grants from the DFG (Sa 196/26-1) to Y.G. and from the DESY 05 641KEB project to P.U. We thank Prof. P. N. Pusey and Dr. A. Mussaid for allowing access to their two-color DLS apparatus and for their kind hospitality at the University of Edinburgh.

JA982407Y

(75) Hoare, M. R.; Pal, P. A. *Adv. Phys.* **1971**, *20*, 161.
(76) Hoare, M. R.; McInnes, J. A. *Adv. Phys.* **1983**, *32*, 791.
(77) MacKay, A. L. *Acta Crystallogr.* **1962**, *15*, 916.